Characterization of highly hydrophobic textiles by means of X-ray microtomography, wettability analysis and drop impact

M Santini[1], M Guilizzoni[2], S Fest-Santini[3], M Lorenzi[4]

[1] Department of Engineering and Applied Sciences, University of Bergamo, viale Marconi 5, 24044 Dalmine, Italy
[2] Politecnico di Milano, Department of Energy, Via Lambruschini 4, 20156 Milano, Italy
[3] Department of Management, Information and Production Engineering, University of Bergamo, viale Marconi 5, 24044 Dalmine, Italy
[4] School of Engineering and Mathematical Sciences, City University London, Northampton Square, London EC1V 0HB, United Kingdom

maurizio.santini@unibg.it

Abstract. Highly hydrophobic surfaces have been intensively investigated in the last years because their properties may lead to very promising technological spillovers encompassing both everyday use and high-tech fields. Focusing on textiles, hydrophobic fabrics are of major interest for applications ranging from clothes to architecture to environment protection and energy conversion. Gas diffusion media – made by a gas diffusion layer (GDL) and a micro-porous layer (MPL) – for fuel cells are a good benchmark to develop techniques aimed at characterizing the wetting performances of engineered textiles. An experimental investigation was carried out about carbon-based, PTFE-treated GDLs with and without MPLs. Two samples (woven and woven-non-woven) were analysed before and after coating with a MPL. Their three-dimensional structure was reconstructed and analysed by computer-aided X-ray microtomography (μCT). Static and dynamic wettability analyses were then carried out using a modified axisymmetric drop shape analysis technique. All the surfaces exhibited very high hydrophobicity, three of them near to a super-hydrophobic behavior. Water drop impacts were performed, evidencing different bouncing, sticking and fragmentation outcomes for which critical values of the Weber number were identified. Finally, a μCT scan of a drop on a GDL was performed, confirming the Cassie-Baxter wetting state on such surface.

1. Introduction

Engineered surfaces have been gaining more and more importance since the last years, as the ability to finely tune the surface properties, at least in part independently from the bulk material properties, may lead to very promising technological applications. Among the different surface properties, hydrophobicity and super-hydrophobicity have been intensively investigated because water repellency, low adhesion, low friction, high restitution coefficient may offer potential benefits in a wide range of fields from everyday use to high-tech applications (e.g. self-cleaning coatings, water repulsion and prevention of ice formation, reduced friction and directional flow, capillary devices in micro-electromechanical systems and microfluidic devices). An important sub-topic is the study of highly hydrophobic textiles (cloths, felts, papers), that is of major interest for applications ranging from manufacturing of consumer goods to Architecture and Civil Engineering, to Design, environment

protection and energy conversion (clothes, umbrellas, tents, tensile structures and coverings, innovative surfaces with peculiar properties – e.g. conductive or antibacterial – membranes and diffusion layers) [1–4]. Within the latter field, gas diffusion media (GDMs) – made by gas diffusion layers (GDLs) and micro-porous layers (MPLs) – for fuel cells [5,6] are a very good benchmark to develop techniques aimed at characterizing the wetting performances of engineered textiles.
Hydrophobicity obviously depends on the intrinsic wettability of the material, related to its surface energies in contact with water and with air (or more in general with the wetting liquid and the surrounding ambient – gas, vapor or another immiscible liquid). Polytetrafluoroethylene (PTFE) and other fluoropolymers may grant contact angles with water higher than 110° [7], but unfortunately the known materials cannot at present reach the so-called super-hydrophobicity (contact angles higher than 150° and contact angle hysteresis under 10°) for smooth surfaces [8]. Hence, the actual strategy for obtaining super-hydrophobicity must also include a proper design of the morphology of the surface, aimed at increasing the specific surface of the material and at getting a suitable roughness (possibly a two-scale hierarchical or fractal roughness, mimicking natural super-hydrophobic surfaces [9–11]). It is necessary to reach the so-called Cassie-Baxter wetting state [12], a composite wetting regime in which the drop does not fill the grooves in the surface texture. For textiles, another aspect to be considered is the fact that the drop may be lift by the fibers protruding from the surface, without truly touching the same. It thus experiences a sort of extreme Cassie-Baxter effect which is not, however, really due to the surface in itself [13]. Regrettably, the Cassie-Baxter wetting state – also known as the ‘‘fakir’’ state [14] – is unstable and for impacting drops over a certain impact velocity a transition occurs towards the Wenzel wetting behavior [15], in which the drop completely fills the grooves (and super-hydrophobicity cannot be reached). For some applications, e.g. GDMs, the behavior in contact with sessile drops is the most representative of real conditions. Even if some authors [16] questions the effective validity of the “external” contact angles (static, maximum advancing and minimum receding) for the prediction of in-pore phenomena, the contact angle and contact angle hysteresis are still the most used "lumped parameters” to provide valuable information about the liquid-surface interaction. For other applications, e.g. for clothes, umbrellas and architectural surfaces, the response to impacting drops is the most representative. Studies about the latter are available in the literature, but almost only concerning smooth surfaces or surfaces where the super-hydrophobic behavior is obtained by regular patterns of micro- and nano- pillars [17] or square posts [18]. On these surfaces four different outcomes of the impact are reported: deposition, sticking, rebound and fragmentation [17,18] and critical velocities separating these outcomes are given. The same outcomes are reported, but at different impact velocities, for surfaces that are made hydrophobic by suitable coatings: on porous super-hydrophobic polymer surface, transitions limits for rebound and fragmentation is determined for significantly lower Weber ($We = \rho V^2 D / \sigma$, where ρ is the density, V is the impact velocity and σ is the surface tension) numbers: 60 [19] in confront to about 400 [20], even if the static contact angle values and hysteresis were similar to the uncoated, micro-structured surfaces. There is on the contrary a lack of information about the correlation between the static and dynamic wetting behavior for surfaces characterized by a complex, three-dimensional structure, as textiles are. The aim of the present study is to partially fill such gap by performing an analysis that combines information about the surface structure, topology and roughness (by means of computer-aided X-ray microtomography, μCT), static and dynamic wettability analyses (by means of a modified axisymmetric drop shape analysis technique) and water drop impacts (by means of high speed imaging), on pseudo-isotropic non regular rough substrates having different morphologies.

2. Investigated surfaces

As representative examples of engineered textiles, gas diffusion media (GDMs) for proton exchange membrane fuel cells (PEMFC) and direct methanol fuel cells (DMFC) were selected. Such layers are used in the fuel cells to reduce the problems of water flooding and methanol cross-over. They consist of a gas diffusion layer (GDL) – usually made of porous carbon paper or carbon cloth, wet-proofed

with PTFE or other fluoropolymers – additionally coated (to increase the performances) with a thin microporous layer (MPL) – made by a mixture of carbon powder, PTFE and other additives [21,22].

Four surfaces were considered in this work: two commercial substrates (SEAL SCCG5N carbon cloth, named CC in the following, and SIGRACET 10CA carbon woven–non-woven, named WNW in the following) analyzed as they are and after coating with a carbon and PTFE microporous layers (coated surfaces will be named CC40 and WNW40 in the following). Full details about the surfaces and the MPL preparation can be found in [5]. All of them have a pseudo-isotropic surface structure, but with different characteristics. Figure 1 shows some examples of the investigated surfaces, including some common issues that may occur in their preparation.

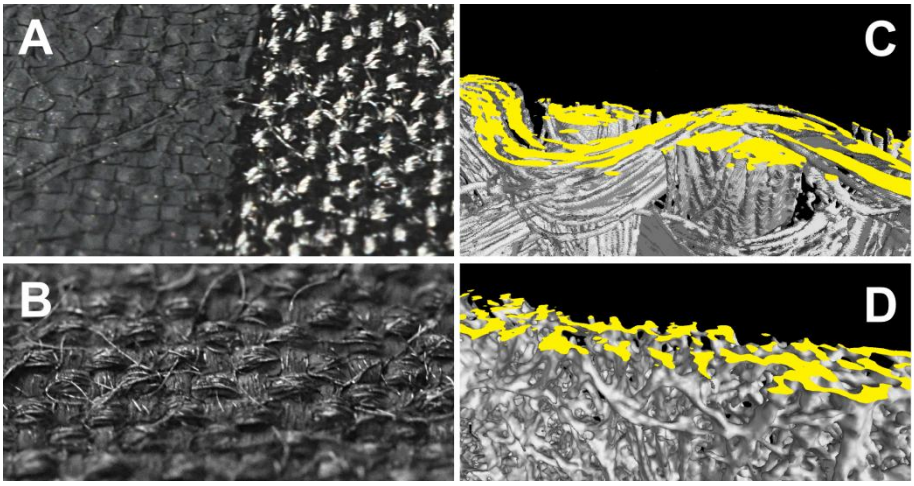

Figure 1. Examples of the investigated surfaces: (A, right part) uncoated CC; (A, left part): CC coated with a thick MPL showing diffuse cracking; (B) CC surface coated with a very thin MPL that is not able to completely cover the CC warp-and-weft structure and protruding fibers; (C) μCT reconstruction of uncoated CC; (D) μCT reconstruction of uncoated WNW.

3. Surface analysis

The four investigated layers were preliminarily observed using a SEM microscope [5], obtaining images characterized by a very high resolution and quality; the disadvantage is that such visualization is only two-dimensional and cannot be used to reconstruct the three-dimensional structure. The latter can on the contrary be obtained by computer-aided X-ray microtomography (μCT) [23-25], that was therefore used in this work to describe the surfaces both qualitatively and by means of suitable quantitative parameters, namely Wenzel roughness ratio, lift and complexity. The first one is defined as the ratio between the actual surface area and the top-view surface area; for the Wenzel wetting state, it also corresponds to the ratio between the real and apparent wetted areas. For each sample, a 3D digital volume was reconstructed by μCT with a resolution between 4 and 8 μm, from which the surface was extracted using a threshold calculated on the basis of the whole 3D volume intensities and saved in stereolitography format (STL) as a triangle mesh. Figure 2 shows two examples of the acquired layers: the woven CC (Fig. 2A) and the woven-non-woven WNW (Fig. 2B), also evidencing the top surface. The extracted surfaces were then sliced, and a contour following technique was implemented to follow the surface profile also within the caves that have some hidden parts when seen from above, but that in the Wenzel assumption are considered as filled with liquid. This approach was carried out on the binary version of each of the vertical, 1-voxel thick, slices of the reconstructed volume. Using the same slice-based approach, the two other surface parameters – lift and complexity – were also calculated. In this case, 40 horizontal lines were analysed for each slice, at depths uniformly spaced between the minimum and maximum height of each slice. More specifically, the surface lift

along each investigated line is the ratio between the number of pixels belonging to the layer and the total length in pixels of the layer along that line. Concerning the surface complexity, it is calculated as the number of transitions between pixels belonging to the layer and pixels belonging to cavities (or vice versa) over the total length in pixels of the layer along that line. It thus counts the number of layer/air or air/slayer interfaces along the chosen line, with an approach completely analogous to the one used for two-phase flow [26,27].

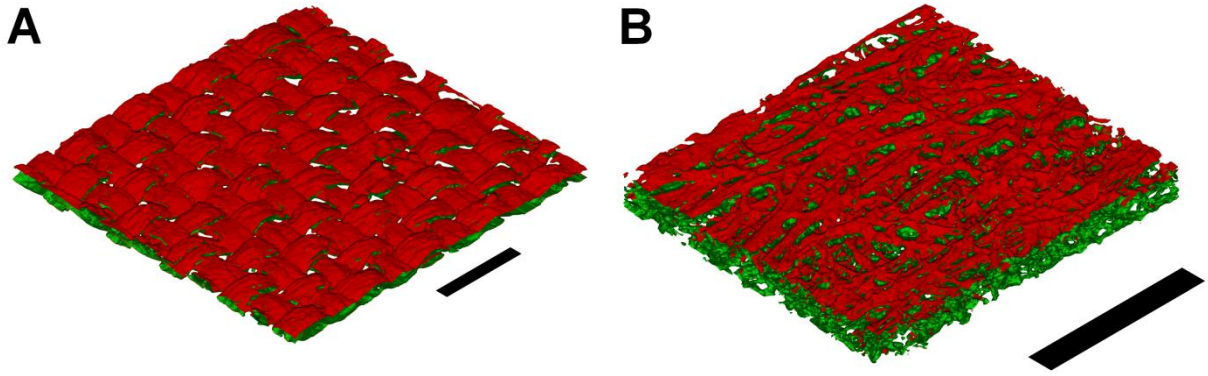

Figure 2. Two clippings from the CC (A) and WNW (B) reconstructed samples, showing in red the facets that are visible in a top view. Black bars represent 1 mm.

Thus lift and complexity profiles were obtained as functions of the height, both as single-slice profiles and as profiles averaged on all the slices. The globally averaged values of lift and complexity on the whole surface can also be calculated. Their values are summarized in Table 1. The roughness of the surface was not included among the descriptive parameters, as it would not add much information with respect to the Wenzel roughness ratio.

Table 1. Surface parameters (all of them are dimensionless) for the investigated layers (average values and standard deviation).

Surface	Wenzel ratio (-)	Lift (-)	Complexity (-)
CC	1.22±0.11	0.458± 0.008	0.024± 0.128
CC40	1.18±0.09	0.474± 0.106	0.028± 0.009
WNW	2.39±0.26	0.255± 0.059	0.058± 0.012
WNW40	2.32±0.17	0.324± 0.046	0.140± 0.021

The Wenzel roughness ratio is higher for the woven-non-woven samples, due to the fiber irregular arrangement and compression. The variability in the measurements is higher for the WNW cases too, both due to the same aspects and to the greater complexity of the μCT acquisition for such samples. The difference in the Wenzel roughness ratio between the uncoated (GDL) and coated (GDL+MPL) surfaces is very slight, contrarily to what could be expected. The cause may be that even if the MPL acts as a film which levels the unevenness of the substrate, it is not able to cover it completely (see Figure 1B). Figure 3A reports the results in terms of averaged (on all the tomographic slices for a layer) surface lift profiles with depth. The analysis of the lift (see Table 1 for the globally averaged values) evidence how the woven surfaces (CC and CC40) offer a higher lift, due to their more compact structure. In their case, the addition of the MPL does not change significantly the lift profile. It just moves the maximum lift region towards the highest lines, where the compact MPL layer is deposed. On the contrary, for the woven-non-woven surfaces (WNW and WNW40) the MPL increase slightly the lift, moreover it enlarges the region of maximum lift towards the lowest lines. Due to the sparser structure of the base substrate, the MPL soaks it more deeply. This reflects also on the average lift value for WNW40. Surface complexity profiles for CC and WNW are shown in Fig. 3B. WNW shows

a much more complex structure than CC. This is consistent with the fact that from both the SEM and μCT analysis, the woven-non-woven surface appears to be similar to a "mangrove forest", with a lot of unordered fibers that creates a tangle and a maze of tunnels between them. On the contrary, the complexity of the WNW40 surface seems odd: it is much higher than all the others, in contrast with the physical appearance of the coated surface. The extraction of the iso-lift contour lines for the CC and WNW surfaces also reproduces the warp-and-weft structure of the woven CC, which is not present in the WNW.

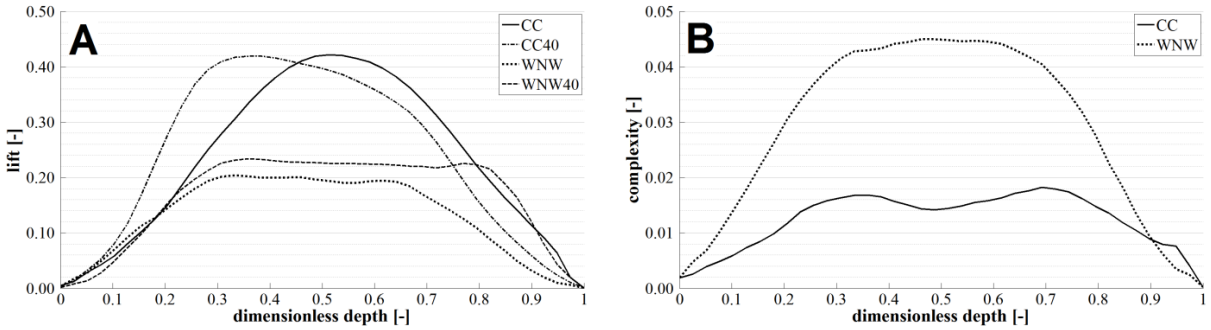

Figure 3. Averaged lift (A) and complexity (B) profiles for the investigated surfaces.

4. Wettability analysis

Micro-tomography can also be used from the quantitative point of view, calculating contact angles on slices of the reconstructed volume, as reported in [28], but for this work wettability analyses were performed using a conventional optical approach, in terms of static "as placed" [29], advancing and receding contact angles. Static "as placed" contact angles and advancing contact angles were measured by means of a modified version of the axisymmetric drop shape analysis technique [30,31], while receding contact angles are estimated from the previous two using a slightly modified (to adapt it to non-wetting drops) version of the model by Tadmor [29]. Figure 4 shows two examples of drops on the WNW and WNW40 surfaces, with the theoretical Laplace-Young contour superposed to the experimental side-views. Figure 5 shows the results of the experimental tests using box plots for the static and advancing contact angles and single markers for the receding contact angle. The whiskers ends represent minimum and maximum values, while the box body covers the interquartile range of the data. Table 2 summarizes the main statistics of the results. The data spreading is quite high but this could be expected due to the rough and not completely homogeneous nature of the investigated surfaces and to the very high values of the contact angles on the same, which makes the measurement extremely difficult [32]. In terms of median or average contact angles, all the investigated surfaces can be regarded as super-hydrophobic. Solely, the woven-non-woven texture WNW goes below the lower limit of super-hydrophobicity if the estimated standard derivation is deducted from the median contact angle. In terms of contact angle hysteresis, the Cassie-Baxter regime is characterized by low contact angle hysteresis and the surfaces CC, CC40 and WNW40 are, therefore, expected to present liquid-solid interaction in this wetting regime. The low receding angle of WNW should instead indicate that the surface exhibits Wenzel behavior and also raises a doubt on the super-hydrophobic behavior of this surface. It is also interesting to note how for the CC surfaces the coating does not significantly enhance the super-hydrophobicity, while for WNW structured surfaces it seems to modify the wetting regime. An explanation of such difference may be found in the different level of coverage that the coating reaches with respect to the asperities of the base substrate: both μCT and SEM analyses of the surfaces [5] show that for woven textiles the coating still follows the warp and weft of the original GDL structure, while on WNW fabrics the coating completely covers the texture of the rough material.

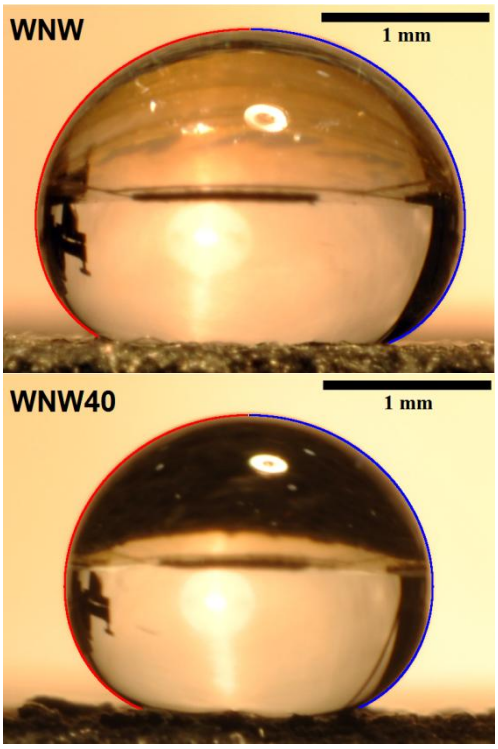

Figure 4. Drop side views on WNW and WNW40, with superposition of the fitted Laplace-Young profile (enlarged to 3 pixels for visualization purposes).

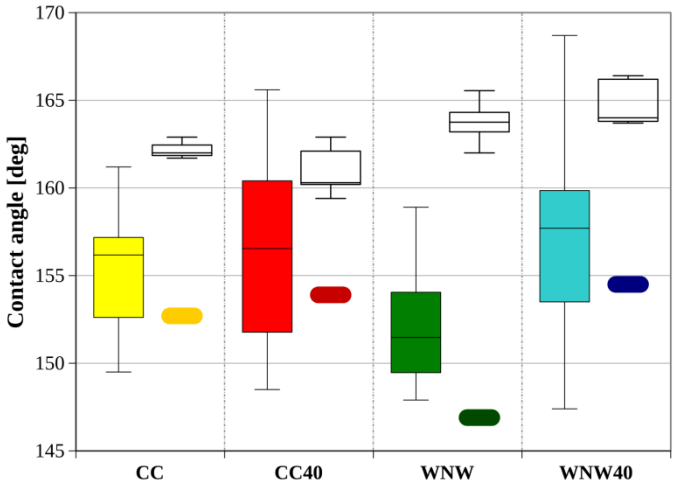

Figure 5. Contact angles of water drops in air on the investigated surfaces: static "as placed" (box plots with coloured background), advancing (box plots with white background) and receding (superellipses markers).

Table 2. Statistical summary of the measured contact angles.

Surface	Median [deg]	Avg. [deg]	Std. dev. [deg]
"As placed" contact angles			
CC	156	155	4.4
CC40	156	156	6.4
WNW	152	152	5.0
WNW40	158	157	5.2
Advancing contact angles			
CC	162	161	5.9
CC40	160	161	1.5
WNW	164	166	4.7
WNW40	164	165	1.4
Receding contact angles (by Tadmor model)			
CC	CC40	WNW	WNW40
153	154	147	154

In previous studies, computer-aided X-ray microtomography (μCT) was also used with very promising results to investigate the real shape of the contact surface and the contact angle profile along the contact line for water drops on smooth and rough surfaces [28,33,34]. Thus, in this study μCT was also used to directly scan a drop on one of the investigate surfaces, to verify the wetting state by a

three-dimensional acquisition of the real system, with micrometric resolution. The non-intrusive, fully 3D nature of microCT allows visualizing the contact region of the drop-surface system. Figure 6 shows the result, after extraction of the drop and CC surfaces as isosurfaces at the proper level of X-ray attenuation. Panel A shows a clipping of the drop and surface to evidence the complexity of the contact between water and GDL, that is further underlined by the extraction of the drop bottom surface in Panel B.

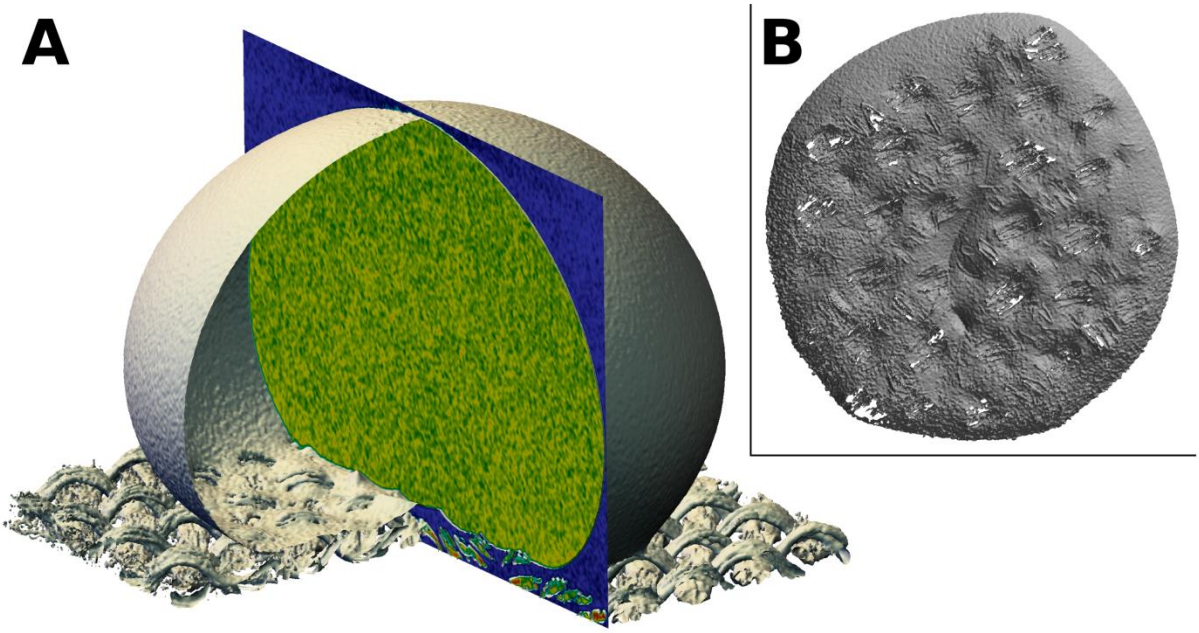

Figure 6. Rendering of drop and CC surfaces extracted as isosurfaces of X-ray attenuation from μCT: A) clipping of the drop and CC surface, B) extraction of the drop bottom surface.

5. Drop impact

Drop impact experiments were carried out using high speed imaging, following a procedure which is described in details in [35,36]. As discussed in the Introduction, four different outcomes of drop impact may be observed, whereby rebound and fragmentation is related to the Cassie-Baxter regime, sticking to the Wenzel regime and deposition could occur for both wetting states [19]. To observe the transition between the different outcomes, the impact velocity was systematically varied by changing the impact height, while the droplet diameter was kept constant to 3.5 mm. The corresponding Weber number was analyzed as a function of a mean contact angle, calculated using the mean advancing and the receding contact angle $(\theta_A + \theta_R)/2$ summarized in Table 1. As an example, two impact events at same impact conditions but on different surfaces are shown in Fig. 7. Figure 8 reports the outcomes of the impact events for all the investigated impact conditions, in terms of contact angle and Weber numbers (open symbols: bouncing/sticking, filled symbols: fragmentation). Experimental data for bouncing and fragmentation from the work of Rioboo et al. [19] and the corresponding contact angle measurements from Rioboo et al. [37] (black triangles) are also reported for comparison. For the surfaces CC, CC40 and WNW40, which behave following the Cassie-Baxter wetting model, transition between bouncing and fragmentation is observed. The minimal required Weber number to observe fragmentation (which will be called "critical Weber number" in the following) and the number of fragmented drops differ for these three surfaces. All the droplets above the critical Weber number are rejected from the surface. The uncoated carbon cloth structure CC and the coated woven-non-woven surface WNW40 exhibit the same critical Weber number of about 50 despite they have different mean contact angles and surface topologies.

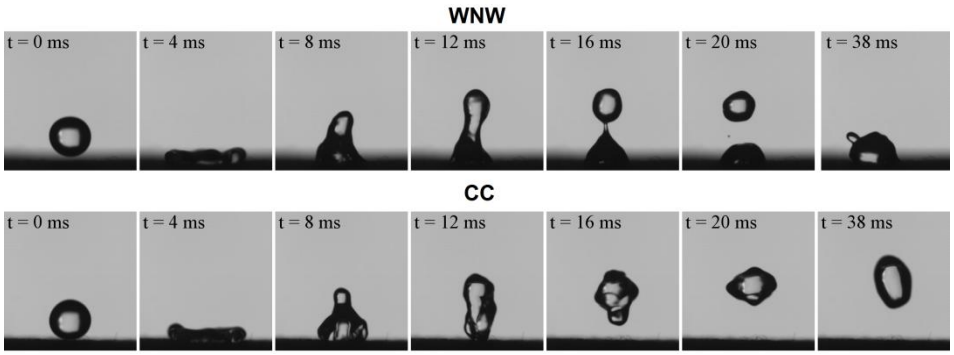

Figure 7. Impact sequence at We = 37.3 on WNW (1st row, with pinning and partial bouncing) and CC (2nd row, with bouncing).

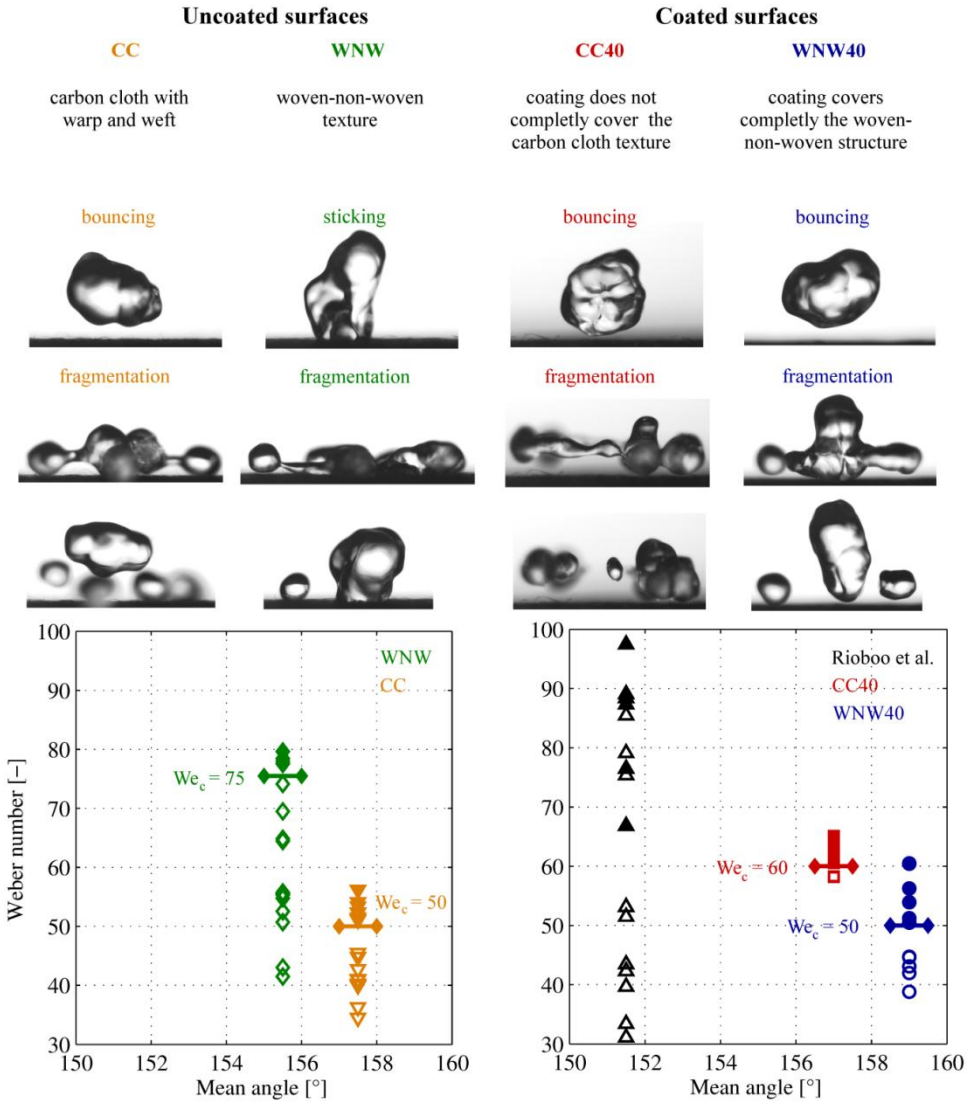

Figure 8. Outcomes of the impact events for different We (open markers: bouncing / sticking, filled markers: fragmentation). Experimental data from the work of Rioboo et al. [19,37] (black triangles) are also reported for comparison.

The CC texture seems to feature the highest lift, whereby the coated woven-non-woven surface WNW40 features the highest observed mean contact angle. However, the number of fragmented drops is higher for the CC substrate. Comparing the two coated structures CC40 and WNW40, transition between bouncing and fragmentation is shifted to higher critical Weber numbers with decreasing mean contact angle. This tendency is confirmed by the experimental results of Rioboo et al. [19,37], which

are also shown in Figure 8 for comparison. The critical Weber number is found to be about 60 for the coated carbon cloth structure CC40. It is worth noting that the carbon cloth structures CC and CC40 feature different critical Weber numbers despite they have similar contact angles. Thereby, it is assumed that the observed effects are caused by the topology modifications, which affect the impact behavior more than the wettability. For the woven-non-woven surface WNW, whose low receding contact angle indicates Wenzel wetting characteristics, sticking is observed for Weber numbers below the critical one of about 75. Above this limit, fragmentation is found. Nevertheless, contrarily to what happens with the other investigated surfaces, the fragmented drops still stick on the surface and thereby seem to behave following Wenzel wetting model, as they do below the critical Weber number. The cause of such behavior has probably to be searched in the peculiar morphology of the WNW surface: its uncoated tangle of unordered and in part protruding fibers entangles the drop, thus preventing its rebound.

Conclusions

The wettability and interactions with sessile and impacting drops of carbon-based, PTFE-treated, surfaces used as GDL and GDM for fuel cells were investigated by joint use of optical techniques for contact angle measurement and drop impact analysis, and X-ray microtomography for surface characterization and direct visualization of the drop-surface couples. Given the rising importance of super-hydrophobic surfaces and engineered textiles, obtaining thorough and reliable information about the surface structure and wetting behavior is of high interest in a wide range of fields, from improvement of consumer goods to architectural and industrial applications. A woven and a woven-non-woven GDLs, both as they are and after coating with a MPL, were analyzed. Even if a deeper investigation is still needed to fully understand some of the outcomes of drop impacts on these kinds of surfaces and the spreading of the measured contact angles is significant, the combined use of such information gave generally consistent results (also in good agreement with literature data). More specifically, the woven-type surfaces, both uncoated and coated, and the coated woven-non-woven surface appear to feature a Cassie-Baxter super-hydrophobic behavior, while the uncoated woven-non-woven surface showed a very high static contact angle, but also a large contact angle hysteresis, more typical of a Wenzel wetting state. The woven-non-woven sample showed also that a surface coating of sufficient thickness, which hides the texture of the base substrate, seems to grant a significant enhancement of the contact angles, probably also changing the governing wetting regime. For coated super-hydrophobic textures, the transition between bouncing and fragmentation is shifted to lower Weber numbers with increasing contact angles. Finally, a microtomographic scan of a drop on a woven surface was acquired, to directly verify the real wetting state. The results confirmed the hypotheses, as the drop on such surface is in a Cassie-Baxter state, with very evident air pockets under its bottom.

Funding sources and acknowledgements

S. Fest-Santini acknowledges funding by *Pro Universitate Bergomensi* within their internationalization projects.

The investigated MPLs were prepared and coated on the GDLs by the Materials for Energy and Environment (MAT4EN^2) group, Dipartimento di Chimica, Materiali e Ingegneria Chimica "G. Natta", Politecnico di Milano. Their contribution is gratefully acknowledged.

References

[1] Shuhui Li, Jianying Huang, Zhong Chen, Guoqiang Chen and Yuekun Lai 2017 *J. Mater. Chem. A* **5** 31–55
[2] Sohyun Park, Jooyoun Kim and Chung Hee Park 2015 *J. Eng. Fiber. Fabr.* **10**(4) 1-18
[3] Latthe S S, Gurav A B, Maruti C S and Vhatkar R S 2012 *J. Surface Engineered Materials and Advanced Technology* **2** 76-94
[4] Xue C-H, Chen J, Yin W, Jia S-T and Ma J-Z 2012 *Appl. Surf. Sci.* **258**(7) 2468–72

[5] Gallo Stampino P, Cristiani C, Dotelli G, Omati L, Zampori L, Pelosato R and Guilizzoni M 2009 *Catal. Today* **147S** S30–S35
[6] Gallo Stampino P, Balzarotti R, Cristiani C, Dotelli G, Guilizzoni M and Latorrata S 2013 *Chemical Engineering Transactions* **32** 1603–08
[7] Lee S, Park J-S and Lee T R 2008 *Langmuir* **24** 4817–26
[8] Arkles B, Pan Y and Kim Y M 2009 The Role of Polarity in the Structure of Silanes Employed in Surface Modification, in Mittal K L, Silanes and Other Coupling Agents, **5**(1) Brill K NV, Leiden, Netherlands 51-64
[9] Guo Z, Liu W and Su B-L 2011 *J. Colloid Interf. Sci.* **353**(2) 335–355
[10] Kang M, Jung R, Kim H-S and Jin H-J 2008 *Colloid Surface A* **313–314** 411–414.
[11] Shibuichi S, Onda T, Satoh N and Tsujii K 1996 *J. Phys. Chem*. **100** 19512–17
[12] Cassie A B D and Baxter S 1944 *T. Faraday Soc.* **40** 546–551
[13] Wang T, Hu X and Dong S 2007 *Chem. Commun.* **18** 1849-51.
[14] Moulinet S and Bartolo D 2007 *Eur. Phys. J. E* **24** 251–260
[15] Wenzel R N 1936 *Ind. Eng. Chem.* **28**(8) 988–994
[16] Gurau V, Bluemle M J, De Castro E S, Tsou Y-M, Mann J A Jr and Zawodzinski T A Jr 2006 *J. Power Sources* **160** 1156–62
[17] Bartolo D, Bouamrirene F, Verneuil É, Buguin A, Silberzan P and Moulinet S 2006 *Europhys. Lett.* **74**(2) 299–305
[18] Smyth K, Paxon A, Kwon H-M, Deng T and Varanasi K K 2010 Dynamic wetting on superhydrophobic surfaces: droplet impact and wetting hysteresis Thermal and Thermomechanical Phenomena in Electronic Systems (ITherm), 12th IEEE Intersociety Conference 2–5 June 2010
[19] Rioboo R, Voué M, Vaillant A and De Coninck J 2008 Drop Impact on porous superhydrophobic polymer surfaces *Langmuir* **24** 14074–77
[20] Reyssat M, Pépin A, Marty F, Chen Y and Quéré D 2006 Bouncing transition on microtextured materials *Europhys. Lett.* **74**(2) 306–312
[21] Guilizzoni M, Gallo Stampino P, Cristiani C, Dotelli G and Latorrata S 2013 *Chemical Engineering Transactions* **32** 1657–62
[22] Latorrata S, Gallo Stampino P, Cristiani C and Dotelli G 2014 *Int. J. Hydrogen. Energ.* **39**(10) 5350 – 57
[23] James J P, Choi H-W and Pharoah J G 2012 *Int. J. Hydrogen. Energ.* **37** 18216–30
[24] Sasabe T, Inoue G, Tsushima S, Hirai S, Tokumasu T and Pasaogullari U 2012 *ECS Transactions* **50**(2) 735–744
[25] Santini M, Guilizzoni M, Lorenzi M, Atanassov P, Marsili E, Fest-Santini S, Cristiani P and Santoro C 2015 *Biointerphases* **10**(3) 031009 1-9
[26] Guilizzoni M *Int. J. Multiphas. Flow* **51** 1–10
[27] Arosio S and Guilizzoni M 2006 *J. Visual.-Japan* **9** 275–282
[28] Santini M, Guilizzoni M and Fest-Santini S 2013 *J. Colloid Interf. Sci.* **409** 204–210
[29] Tadmor R 2004 *Langmuir* **20** 7659–64
[30] del Rio O I, Neumann A W 1997 *J. Colloid Interf. Sci.* **196**(2) 136–147
[31] Guilizzoni M 2011 *J. Colloid Interf. Sci.* **364** 230–236
[32] Extrand C W and Moon S I 2010 *Langmuir* **26**(22) 17090–99
[33] Santini M. and Guilizzoni M 2014 *Colloids and Interface Science Communications* **1** 14–17
[34] Santini M, Guilizzoni M, Fest-Santini S and Lorenzi M 2015 *Rev. Sci. Instrum.* **86** 023708
[35] Santini M, Fest-Santini S and Cossali G E 2013 *Exp. Fluids* **54** 1593–07
[36] Santini M, Fest-Santini S and Cossali G E 2017 *Eur. J. Mech. B-Fluid* **62** 21–31
[37] Rioboo R, Voué M, Vaillant A, Seveno D, Conti J, Bondar A I, Ivanov D A and De Coninck J 2008 *Langmuir* **24**(17) 9508–14